Applied Catalysis B: Environmental 322 (2023) 122089

Contents lists available at ScienceDirect

Applied Catalysis B: Environmental

journal homepage: www.elsevier.com/locate/apcatb

Rh-Pd/TiO_2 as bilateral catalysts for reductive and oxidative degradation of fluorinated pharmaceutical contaminants

Jaehyeong Park [a], Sungjun Bae [b], Yongju Choi [a], Jong Kwon Choe [a,*]

[a] Department of Civil and Environmental Engineering and Institute of Construction and Environmental Engineering, Seoul National University, 1 Gwanak-ro Gwanak-gu, Seoul 08826, Republic of Korea
[b] Department of Civil and Environmental Engineering, Konkuk University, 120 Neungdong-ro, Gwangjin-gu, Seoul 05029, Republic of Korea

ARTICLE INFO

Keywords:
Fluconazole
Bilateral catalysts
Fluorinated pharmaceutical
Catalytic treatment
Sequential reduction and oxidation

ABSTRACT

This study is the first to investigate the applicability of a single catalyst (Rh-Pd on TiO_2 support) that enables radical-based advanced oxidation and reductive hydrogenation of fluconazole, a fluorinated pharmaceutical. The catalyst was characterized using characterization techniques (e.g., TEM-EDX, XPS), and its ability for bilateral treatment of fluconazole was investigated using H_2 as reductant for reduction and peroxymonosulfate to generate radicals for oxidation. The catalyst was capable of efficiently degrading fluconazole in both directions with k_{obs} of 0.60 ± 0.09 L/(min•g_{cat}) for oxidation and 0.0191 ± 0.0005 L/(min•g_{cat}) for reduction. Compared to oxidative treatment only, minimal formation of fluorine-containing transformation products was achieved through sequential reduction and oxidation treatment, suppressing the numbers from 18 to 3. Results from this study has shown the capability of Rh-Pd/TiO_2 as bilateral catalyst, opening up the new and promising possibility of a single catalyst that triggers both oxidative and reductive treatments for water treatment and other environmental applications.

1. Introduction

A variety of organofluorine compounds with fluorinated functional groups (e.g., alkyl-F, aryl-F, aryl-CF_3, and aryl-OCF_3) have recently been at the forefront of the pharmaceutical [1,2], agrochemical [3,4], and dye industries [5]. This is because the formation of C-F bonds in a molecular framework induces (i) better protection of fluorinated compounds against in vivo metabolism (e.g., P450 oxidation) and (ii) bond polarization, which modulates the lipophilicity and pK_a values of the molecule [1,4]. These advantages are intriguing aspects of fluorination, especially in pharmaceutical and agrochemical studies. Hence, fluorination technologies have been intensively developed and improved for syntheses of more effective and metabolically stable drugs and herbicides. With the global population expected to increase from 7 billion to 9.6 billion within 30 years, the demand for increases in drug and crop production also leads to the need for novel fluoro-pharmaceuticals and fluoro-herbicides [1,4]. In recent years, an estimated 20% and 25% of approved drugs and herbicides have been fluorinated [1,4]. However, the continuous success of fluorinated compounds in those areas has resulted in the occurrence of organofluorine compounds in surface waters, soils, and animals at ng/L to μg/L levels, leading to environmental problems and health issues [6]. For example, fluconazole, 2-(2, 4-difluorophenyl)− 1,3-bis-(1*H*-1,2,4-triazol-1-yl)− 2-propanol, is a triazole antifungal drug that is relatively recalcitrant [7] and has been considered an emerging contaminant detected in surface water (1–111 ng/L), wastewater influent (22–570 ng/L), hospital effluent (13 μg/L) [8] and treated effluent (28–140 ng/L) [9,10].

Different treatment technologies, such as chemical oxidation (e.g., Fenton and ozonation) [11–15], photochemical reactions [16,17], photocatalysis [18,19], electrochemical reactions [20] and electron beams [21], have been studied for abatement of fluorinated compounds. However, only a limited number of fluorinated drugs (e.g., fluoro-quinolone antibiotics) have been investigated, resulting in a lack of knowledge regarding degradation pathways for oxidation of fluorinated compounds. Additionally, these oxidative treatment technologies have several challenges in the treatment of fluorinated chemicals, such as (i) partial oxidative defluorination [13] and (ii) formation of a large number of byproducts containing fluorine [22]. These problems are exacerbated by the presence of complex water matrices on the field scale, which can induce early termination of the reaction due to radical scavenging and attenuation of radiation [23]. Thus, potentially toxic and recalcitrant fluorinated species could remain in the water even after

* Correspondence to: Seoul National University, 1 Gwanak-ro, Gwanak-gu, Seoul 08826, Republic of Korea.
E-mail address: jkchoe@snu.ac.kr (J.K. Choe).

https://doi.org/10.1016/j.apcatb.2022.122089
Received 24 June 2022; Received in revised form 31 August 2022; Accepted 18 October 2022
Available online 20 October 2022

treatment.

Reductive treatment of fluorinated compounds in water has also been investigated in a limited number of studies. Under H_2 feed conditions, Pt-group noble metal catalysts (e.g., Ru, Rh, Pd, and Pt) were shown to effectively generate H_{ads}-M (H_{ads} = adsorbed surface hydrogen, M = noble metal) for reductive defluorination and hydrogenation of fluorinated compounds [24–26]. In our previous study, almost complete defluorination of aryl fluorides was also observed with Pt-group metal catalysts, and defluorination and degradation kinetics were enhanced after introduction of the second metal [24]. Defluorination was often the initial steps of the degradation pathways during reductive treatment. Therefore, it can be hypothesized that if fluorinated compounds undergo reductive pretreatment followed by oxidative treatment, the generated defluorinated intermediates will be the main oxidation targets, and the formation of fluorinated intermediates could be significantly suppressed. However, implementation of such a hybrid process in water treatment must overcome significant hurdles, such as the complexity and difficulty of reactor design and additional separation processes (e.g., separation of catalysts from water). Herein, the use of a single catalyst in a sequential process was proposed for simplicity of design and ease of operation. Recently, it was reported that noble metals effectively activate peroxymonosulfate (PMS) to generate $SO_4^{\cdot-}$ and $^{\cdot}OH$, which are strong oxidants with oxidation potentials of 2.5–3.1 V and 1.7–2.5 V, respectively [27–29]. Therefore, Pt-group metal catalysts could mediate both the reduction and oxidation of organofluorine compounds and other halogenated contaminants. However, mono- or bimetallic catalysts that induce both reductive and oxidative degradation of organic compounds in water have not been reported and developed to date.

The present study was designed to explore applicability of mono- (i.e., Rh, Pd, and Pt) and bimetallic catalysts (i.e., Rh-Pd, Rh-Pt, and Pd-Pt) deposited on TiO_2 supports as bilateral catalysts for reductive and oxidative treatments of fluorinated pharmaceuticals, using fluconazole as a model compound. TiO_2 was used as a catalyst support for its excellent chemical stability (e.g., noncorrosive property), high durability, water insolubility, and low cost. The specified objectives of this study are (i) to characterize the physicochemical properties of the catalysts using a series of characterization techniques, including field emission transmission electron microscopy (FE-TEM), energy-dispersive X-ray spectroscopy (EDX), temperature programmed reduction (TPR), the Brunauer–Emmett–Teller (BET) method, H_2-pulse chemisorption analysis, and X-ray photoelectron spectroscopy (XPS), (ii) to investigate catalytic reduction and oxidation kinetics, degradation pathways and intermediate formation, (iii) to explore the applicability of sequential reduction and oxidation, and (iv) to elucidate three reaction processes (reduction, oxidation, and sequential reduction and oxidation) and associated degradation mechanisms using density functional theory (DFT) calculations.

2. Materials and methods

2.1. Chemical reagents and catalyst preparation

Information of all chemicals used for the synthesis of bimetallic catalysts, reduction and oxidation of fluconazole, and measurement of fluconazole and its intermediates is provided in the Appendix (**Text A.1**). Monometallic catalysts (Rh, Pd, and Pt) and bimetallic catalysts (Rh-Pd, Rh-Pt, and Pd-Pt) supported on TiO_2-rutile (<100 nm) were prepared using the impregnation method [24,30]. TiO_2-rutile (<100 nm) powder (1.0 g) was added to 80 mL of deionized water (DIW) in a polypropylene bottle, and the suspension was sonicated for 5 min. Pd, Rh, and Pt precursor solutions were prepared, and the target amount of precursor solution was added into the suspension. For Rh-Pd bimetallic catalysts, two precursor solutions were added simultaneously into the suspension. The suspension was then maintained under stirring at 500 rpm for 2 h at room temperature and then dried in an oven at 105 ℃ for 24 h. The dried powder was transferred into an alumina crucible and calcined at 350 °C for 2 h in a muffle furnace (MF-10, Jeio-Tech, Korea) to strengthen the doping of mono- or bimetals on the surface of TiO_2-rutile (<100 nm). After calcination, Rh-Pd/TiO_2-rutile (<100 nm) (afterward denoted as Rh-Pd/TiO_2) was ground into fine particles, transferred into glass vials and stored prior to use. Before each catalytic reduction/oxidation experiment, 0.1 g of the catalyst was mixed with 15.0 mL of DIW and sonicated for 30 s. Then, an aqueous solution of 50 mM $NaBH_4$ (20 mL) was added dropwise into the suspension under continuous stirring at 1000 rpm for 15 min. $NaBH_4$ was used to reduce metal catalysts on the surface of TiO_2-rutile (<100 nm). The catalysts were washed with deaerated DIW twice to remove residual $NaBH_4$ and immediately used for batch experiments. Rh-Pd bimetallic catalysts supported on different support materials (i.e., TiO_2-rutile (<5 μm), TiO_2-anatase, TiO_2-mixture of rutile and anatase (<100 nm), TiO_2--brookite (<100 nm)) were prepared similarly.

2.2. Catalytic oxidation and reduction kinetic experiments

Oxidative degradation of fluconazole (32.65 μM) was performed in a magnetically stirred 120 mL glass reactor containing aqueous suspensions of 0.2 g/L or 0.4 g/L Rh-Pd/TiO_2 and 0.5 mM PMS. The reaction suspensions were typically buffered at a pH of approximately 7.0 using 0.93 mM bicarbonate buffer. Only marginal changes in pH were observed over the course of the oxidation reactions [28]. Sample aliquots were periodically withdrawn from the reaction using a 3 mL syringe (Korea Vaccine Corp., Korea) and filtered through a 0.2 μm PTFE filter (Whatman, USA). Then, 1.0 mL of the filtrate was transferred into a 2 mL glass vial. Then, 100 μL of LC–MS grade methanol was immediately spiked into the vial to quench radicals.

Kinetic experiments for catalytic reduction of fluconazole were also conducted in a glass reactor (120 mL). Activated Rh-Pd/TiO_2 (20 or 40 mg) was injected to 98 mL of deaerated DIW in the reactor and sonicated using a bath sonicator for 1 min to ensure complete dispersion of catalyst particles. The suspension was stirred continuously at 1000 rpm. After the reactor was tightly sealed with an aluminum crimp cap lined with a rubber septum, H_2 gas was purged for 20 min before initiation of the reaction. In order to initiate the catalytic reaction, 2.0 mL of a stock solution of fluconazole was injected to give an initial concentration of 32.65 μM in the presence of continuous flow of H_2 (200 mL/min). Sample aliquots were periodically withdrawn from the reaction using a 3 mL syringe, filtered through a 0.2 μm PTFE syringe filter, and transferred into vials before analysis.

The reactivities of monometallic catalyst (Rh, Pd, and Pt) and bimetallic catalysts (Rh-Pd, Rh-Pt, and Pd-Pt) supported on TiO_2 for reduction and oxidation of fluconazole were also investigated under the same conditions. Additional experiments were conducted to investigate the effects of Pd loading, Rh loading, and catalyst dosage on the reduction and oxidation of fluconazole by using five different Pd loadings (0%, 0.5%, 1.0%, 1.5%, and 2.0%) and Rh (0%, 0.5%, 1.0%, 1.5%, and 2.0%) and different concentrations of Rh-Pd/TiO_2 catalyst (0.01, 0.05, 0.1, 0.2 and 0.4 g/L). Scavenging tests using methanol ([methanol]/[fluconazole]$_0$ = 250) and *tert*-butanol ([*tert*-butanol]/[fluconazole]$_0$ = 250) were carried out to examine the activation of PMS and the production of oxidative species ($SO_4^{\cdot-}$ and $^{\cdot}OH$) by Rh-Pd/TiO_2.

Sequential reduction and oxidation of fluconazole was also conducted using Rh-Pd/TiO_2 (0.4 g/L). Catalytic reduction of fluconazole was conducted similarly. After the reaction, 1.0 mL was taken from the reactor for analysis of the remaining fluconazole and its intermediates. Then, the reaction mixture was purged with O_2 for 30 min to remove H_{ads}-Pd and H_{ads}-Rh. Then, 1.0 mL of PMS solution was spiked into the reactor to initiate the oxidation reaction. Sample aliquots were withdrawn with syringes at specified time intervals, filtered, and quenched with methanol by the method described above. The reaction temperature was kept at 25 ± 0.5 ℃. All data were obtained from experiments performed in triplicate.

2.3. Analytical techniques and methods

The concentrations of the fluconazole and byproducts were determined by single quadrupole liquid chromatography–mass spectrometry (LC–MS, 6120DW, Agilent, USA). The relative abundance of intermediates generated during reduction, oxidation, and sequential reduction and oxidation of fluconazole was quantified by using mass spectrometry peak areas. The LC system (1260 Infinity II, Agilent, USA) was equipped with a ZORBAX Extend-C18 column (2.1 × 150 mm, 1.8 μm). Acetonitrile (eluent A) and 0.1% formic acid in water (eluent B) were used for eluting fluconazole. The time profile of gradient used for analysis of fluconazole was initiated at 5% A and 95% B at (0 min). Then, B was reduced to 5% from 0 min to 9 min, maintained at 5% for 1 min, increased to 95% B from 10 min to 11 min, and re-equilibrated from 11 min to 25 min. The injection volume was 5 μL, and the column temperature was set to 30 °C. The elution flow rate was maintained at 0.2 mL/min. Electrospray ionization MS in positive ion mode was used to identify fluconazole (*m/z* 307.1) and its intermediates. The following MS settings were used: drying gas (i.e., N_2) flow rate of 12.0 L/min, nebulizer pressure of 50 psi, drying gas temperature of 350 °C, capillary voltage of 4000 V (positive) and 3500 V (negative), and fragmentor voltages of 110 V.

LC-QTOF-MS analysis was performed using a high-pressure LC instrument (Ultimate3000, Thermo Scientific Inc., USA) coupled to an AB Sciex TripleTOF 5600 + system (AB Sciex, USA) with a Waters Cortex C18 column (2.1 mm × 150 mm, 1.6 μm). Eluents for the mobile phase were prepared from a mixture of 0.1% formic acid in water (eluent A) and 0.1% formic acid in acetonitrile (eluent B) and used with a flow rate of 0.3 mL/min. The column temperature was 30 ℃. The eluent gradient time profile used for analysis was as follows: 95% A at t = 0 min, decreased to 5% to 7 min, held at 5% A from 7 min to 12 min, increased to 95% A from 12 min to 13 min, and re-equilibrated from 13 min to 20 min. The source conditions of the QTOF-MS were as follows: nebulizing gas pressure of 50 psi, heating gas pressure of 50 psi, curtain gas pressure of 25 psi, source temperature of 500 °C, declustering potential of − 60 V, collision energy of 20 ± 10 V, and ion spray voltage floating of 5.5 kV. Mass spectra were obtained via full scan and information-dependent acquisition scanning in the scan range 50–1000 *m/z* and 30–1000 *m/z* for MS and MS/MS, respectively. LC–MS and LC-QTOF-MS analyses were performed to quantify fluconazole and identify the intermediates formed during the reduction, oxidation, and sequential reduction and oxidation processes. The chemical structures of the detected intermediates were proposed based on their accurate full-product ion spectra.

The F^- ion concentration in the solution was quantified using an ion chromatograph (IC, Metrohm, 883 Basic IC plus) equipped with a compact autosampler (Metrohm, 863 Compact IC) and anion column (Shodex IC Anion Sep No. 82504 A). A mixture of Na_2CO_3 (3.2 mM) and $NaHCO_3$ (1 mM) was used as the eluent with a flow rate of 0.7 mL/min. PMS was quantified via a previously reported method utilizing iodine (λ_{max} = 352 nm) formation during the reaction of PMS and iodide [31]. A linear relationship was observed between absorbance at 352 nm and PMS concentration in the range 30 μM to 1000 μM.

The morphologies and metal dispersions of Rh/TiO_2, Pd/TiO_2, and Rh-Pd/TiO_2 were characterized via field-emission transmission electron microscopy equipped with energy dispersive X-ray spectroscopy (FE-TEM/EDX) using a JEOL JEM-F200 (TFEG) instrument (Japan). Prior to analyses, the bimetallic catalysts activated with $NaBH_4$ (in Section 2.2) were rinsed sequentially with deaerated deionized water, 50% deaerated ethanol, and 100% deaerated ethanol, and then dispersed in deaerated ethanol to prevent oxidation. Additionally, the chemical environments of the metal catalysts (Rh and Pd) were characterized via in situ X-ray photoelectron spectroscopy (XPS, Axis-Supra, Kratos Analytical, UK) with Al Kα X-ray (1486.7 eV) radiation at a source power of 75 W. The C 1 s peak at 285 eV was used as the reference for adjusting surface charging effects.

Temperature-programmed reduction (TPR, AutoChemII2920, Micromeritics Instrument Corp., USA) analyses of TiO_2, 1% Rh/TiO_2, 1% Pd/TiO_2, and 1% Rh-1% Pd/TiO_2 catalysts were also performed in the temperature range 50–1000 °C with ramping of 20 °C/min, and 10% H_2/Ar was passed through with a flow rate of 10 mL/min. H_2 pulse chemisorption was also performed to determine the dispersion of metals on the TiO_2-rutile (<100 nm) surface by AutoChemII2920 (Micromeritics Instrument Corp., USA). Mono- and bimetallic catalysts before $NaBH_4$-induced activation were outgassed under vacuum and then reduced under a flow of 10% H_2/Ar for 2 h at 350 °C, then flushed with Ar for 1 h and cooled to 30 °C. Chemisorption tests were performed at 30 °C by pulsing 10% H_2/Ar.

2.4. Density functional theory calculations

Density functional theory (DFT) calculations were performed using the ORCA 4.2.1 software package [32]. The Lee-Yang-Parr correlation functional (B3LYP) method with the def2-SVP basic set [33,34] was used for geometry optimization of fluconazole and intermediates. All calculations were conducted with the RIJCOSX approximation. Initial geometry guesses of fluconazole and TPs were prepared using the Avogadro 1.2.0 program [35]. Specifically, the HOMO (highest occupied molecular orbital) and LUMO (lowest unoccupied molecular orbital) were calculated. In addition, the reactive sites of fluconazole and reduction intermediates were predicted using the Fukui function [36]. The Fukui function is widely used for predicting regioselectivity in radical-involved reactions [36–38], and it is defined as [39]:

$$f(r) = \left[\frac{\partial \rho(r)}{\partial N}\right]_{\nu} \quad (1)$$

$$f_A^+ = q_A(N+1) - q_A(N) \quad (2)$$

$$f_A^- = q_A(N) - q_A(N-1) \quad (3)$$

$$f_A^0 = (q_A(N-1) - q_A(N+1))/2 \quad (4)$$

$\rho(r)$ is the electron density at each point r where the total number of electrons (i.e., N) is changed, and the constant term ν in the partial derivative is the external potential. The visualization of the Fukui function was conducted using ChemCraft (version 1.8). The condensed Fukui function was estimated using the Hirshfeld charge number, which indicates the electron density distribution around each atom [36]. Hence, $q_A(N)$ is the atomic charge of atom A when N electrons are present. $q_A(N-1)$ and $q_A(N+1)$ are the charges of the atom on the system with $N-1$ and $N+1$ electrons, respectively [40]. f^+ and f^- describe the preferences of certain atoms for nucleophilic and electrophilic attack, respectively, and a higher f^0 indicates more reactivity toward radical attack [37,41]. Eq. (4) was used to obtain f_A^0, which is the average of f^+ and f^- [39].

3. Results and discussion

3.1. Catalyst characterization

The physicochemical properties of the Rh-Pd/TiO_2 catalyst are shown in Table 1 and Fig. 1. The BET specific surface area of Rh-Pd/TiO_2 was 27.4 m^2/g, and loading of the Rh and Pd nanoparticles did not change the overall surface area of the catalyst significantly from that of the TiO_2 support (i.e., 27.8 m^2/g). The N_2 adsorption-desorption isotherms and distributions of pore size in the Rh-Pd/TiO_2 catalyst (Fig. A.1) showed that the support generally had a mesoporous nature. FE-TEM/EDX analyses were also performed to characterize Pd/TiO_2, Rh/TiO_2, and Rh-Pd/TiO_2 (Fig. 1, Fig. A.2 and Fig. A.3). FE-TEM images showed that TiO_2-rutile support particles had rod (or oval) shapes with 20–50 nm thickness and 40–80 nm length, and these particles were mostly agglomerated (Fig. A.2a, 2b, and 2c). Many nanosized spherical

Table 1
H_2 pulse chemisorption of Pd/TiO_2-rutile (<100 nm), Rh/TiO_2-rutile (<100 nm), and Rh-Pd/TiO_2-rutile (<100 nm).

Catalyst	H_2 cumulative uptake (cm^3/g)	Metal dispersion (%)	Metallic surface area (m^2/g_{metal})	Active particle diameter (nm)	Cubic crystallite size (nm)
Pd/TiO_2-rutile (<100 nm)	0.22	20.88	93.00	5.37	4.47
Rh/TiO_2-rutile (<100 nm)	0.95	86.95	382.70	1.26	1.05
Rh-Pd/TiO_2-rutile (<100 nm)	0.75	35.19	155.83	3.15	2.63

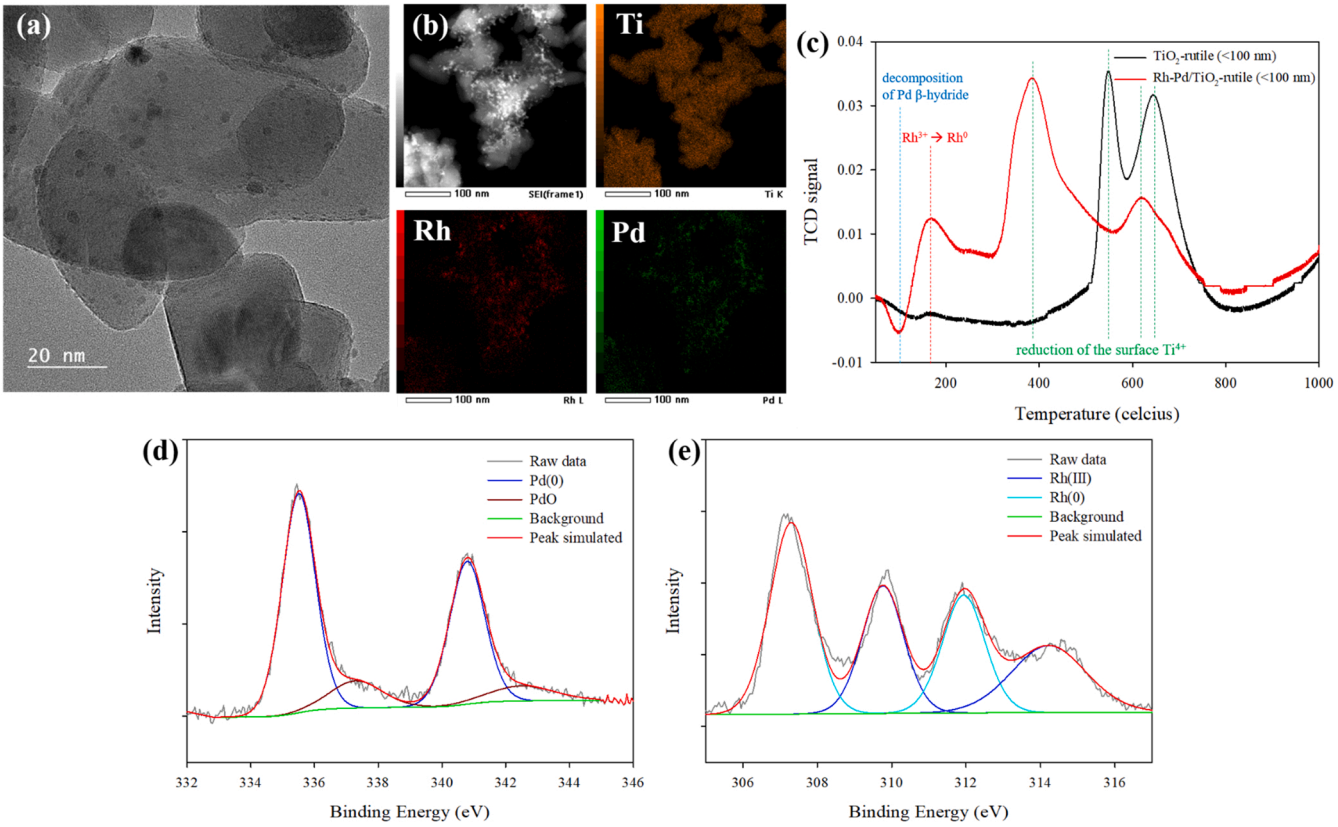

Fig. 1. (a) FE-TEM images and (b) EDS electron mapping images (Ti, Rh, and Pd) of Rh-Pd/TiO_2-rutile (<100 nm), (c) TPR profiles of TiO_2-rutile (<100 nm) and Rh-Pd/TiO_2-rutile (<100 nm), and XPS spectra of (d) Pd (3d) and (e) Rh (3d) for Rh-Pd/TiO_2-rutile (<100 nm) catalysts before reaction.

particles were dispersed on the support surface (Fig. 1a), and EDX mappings of the catalysts showed that Rh and Pd nanoparticles were finely dispersed on the surface and in close proximity (Fig. 1b), which showed that bimetallic catalysts were successfully formed [42,43]. H_2-TPR analysis profiles for the catalysts (Fig. 1c. and A.4) also corroborate the microscopic characterization (detailed discussions on TPR is provided in Section A.2). Using H_2 pulse chemisorption, the metal dispersion and metallic surface area of Rh-Pd/TiO_2 were also quantified as 35.19% and 155.83 m^2/g_{metal}, respectively (Table 1).

The surface Rh and Pd oxidation states of Rh-Pd/TiO_2 were also analyzed by XPS analysis (Figs. 1d, 1e, and Fig. A.5). Before the reaction, the synthesized Rh-Pd/TiO_2 was activated with an aqueous solution of $NaBH_4$ to form metallic Pd and Rh. After activation, occurrence of new doublet peaks at 335.6 (Pd $3d_{5/2}$) and 340.8 eV (Pd $3d_{3/2}$) was observed, indicating the formation of metallic Pd (84.07%) (Fig. 1d and Table 2) [44]. We also observed doublet peaks in the Rh spectrum at 307 eV (Rh $3d_{5/2}$) and 312 eV (Rh $3d_{3/2}$), which correspond to Rh(0) (56.25%) [24] (Fig. 1e and Table 2). The results demonstrated that metallic Pd and Rh nanoparticles are present on the surface of catalysts, which can activate H_2 and PMS during reductive and oxidative degradation experiments of fluconazole, as discussed in the sections below.

Table 2
Oxidation states of metals in Rh-Pd/TiO_2-rutile (<100 nm) catalysts before activation, before reaction, after reduction and oxidation, and after sequential reduction and oxidation.

Metal oxidation state	Before activation (%)	Before reaction (after activation with $NaBH_4$) (%)	After reduction only experiment (%)	After oxidation only experiment (%)	After sequential reduction and oxidation (%)
Pd(II)	85.5	15.93	16.42	38.93	33.96
Pd(0)	14.5	84.07	84.58	61.07	66.03
Rh(III)	100	43.75	48.62	64.23	61.62
Rh(0)	0	56.25	51.38	35.77	38.38

3.2. Catalytic oxidative treatment of fluconazole

3.2.1. Degradation kinetics and fluorine removal

Near complete degradation of fluconazole (>98%) was observed over 180 min with 85.7 ± 4.8% defluorination for the Rh-Pd/TiO_2 catalyst with PMS (Figs. 2a and 2b). No fluconazole degradation occurred with PMS in the absence of catalysts (Fig. 2a), suggesting that, without activation, PMS (E_H = 1.82 V) cannot oxidize fluconazole at pH 7. A bare TiO_2 support with PMS also showed negligible removal of fluconazole in aqueous solution; therefore, fluconazole sorption on the TiO_2 surface can be neglected in this study. Bimetallic Rh-Pd catalysts showed higher catalyst activity (0.60±0.09 L/(min•g_{cat})) than monometallic Pd and Rh catalysts (0.17±0.01 L/(min•g_{cat}) and 0.48±0.02 × 10^{-2} L/(min•g_{cat})) (Fig. A.6(a) and more efficient defluorination (85.7% vs. 57.2% and 24.1%) (Fig. A.6b). Based on these results, TOF values of fluconazole oxidation (3.28 × 10^{-4} s^{-1}) and defluorination (3.68 × 10^{-4} s^{-1}) by Rh-Pd/TiO_2 was estimated (Table A.1). Other monometallic metals (Pt) and bimetallic systems (i.e., Pd-Pt, Rh-Pt) were also investigated but showed lower reactivity than monometallic Pd catalyst (Fig. A.7a). It is interesting to find that the decomposition rate of PMS by Pd/TiO_2 and Rh-Pd/TiO_2 were relatively close (0.014 min^{-1} versus 0.024 min^{-1}). However, the degradation kinetics (i.e., about 3.7 times) and defluorination (i.e., about 1.5 times) of fluconazole in Pd/TiO_2 was much lower than that of Rh-Pd/TiO_2 with the same concentration of PMS (Fig. A.6). Relatively small difference in the rate of PMS decomposition but enhanced degradation and defluorination in fluconazole oxidation suggested that the utilization efficiency of PMS by Rh-Pd ensembles was greatly improved by the synergistic effect between Rh and Pd. These results suggested that reactive species ($SO_4^{\bullet-}$ and •OH) were effectively produced by Rh-Pd and utilized for degradation of both fluconazole and its byproducts. Therefore, it was concluded that the combination of Pd and Rh influenced the catalytic oxidation of fluconazole and byproduct selectivity.

The influences of catalyst support type on oxidative treatment of fluconazole were also investigated (Fig. A.8). The highest catalyst activity and defluorination efficiency were observed for TiO_2-rutile, followed by brookite and anatase (Fig. A.9). The decomposition of PMS also decreased in the same order. When a rutile-phase TiO_2 support with submicron particle sizes (< 100 nm) was compared with the same support exhibiting micron particle sizes (< 5 μm), the TiO_2 support with the smaller particle size showed better catalytic performance (Figs. A.8 and A.9). It is likely that support types and particle sizes influence metal crystalline structures, sizes, and dispersion of Rh-Pd ensembles (Table A.2) and the capacity for PMS activation; among the different supports investigated in this study, the rutile-phase TiO_2-supported catalysts showed the best performance. The influences of catalyst loading (Fig. A.10), PMS dosage (Fig. A.11), bicarbonate ions (Figs. A.12 and A.13), Pd and Rh loading (Fig. A.14 and A.15), initial concentration of fluconazole (Fig. A.16(a)), and natural organic matter (Fig. A.17(a)) on catalytic oxidation of fluconazole were also investigated and are detailed in the Appendix (Text A.3).

After Pd-Rh bimetallic catalysts were used for fluconazole oxidation, changes in their chemical species were analyzed via XPS (Fig. A.5e and A 0.5 f). After their uses, an increase in the peak proportion for Pd^{2+} (16–39%) and a decrease in metallic Pd (84–61%) were observed, indicating partial oxidation of Pd(0). Similarly, partial oxidation of Rh was also indicated by an increase in Rh^{3+} (44–64%) and a decrease in metallic Rh (56–36%). These oxidation state changes in metal species were likely caused by PMS [28].

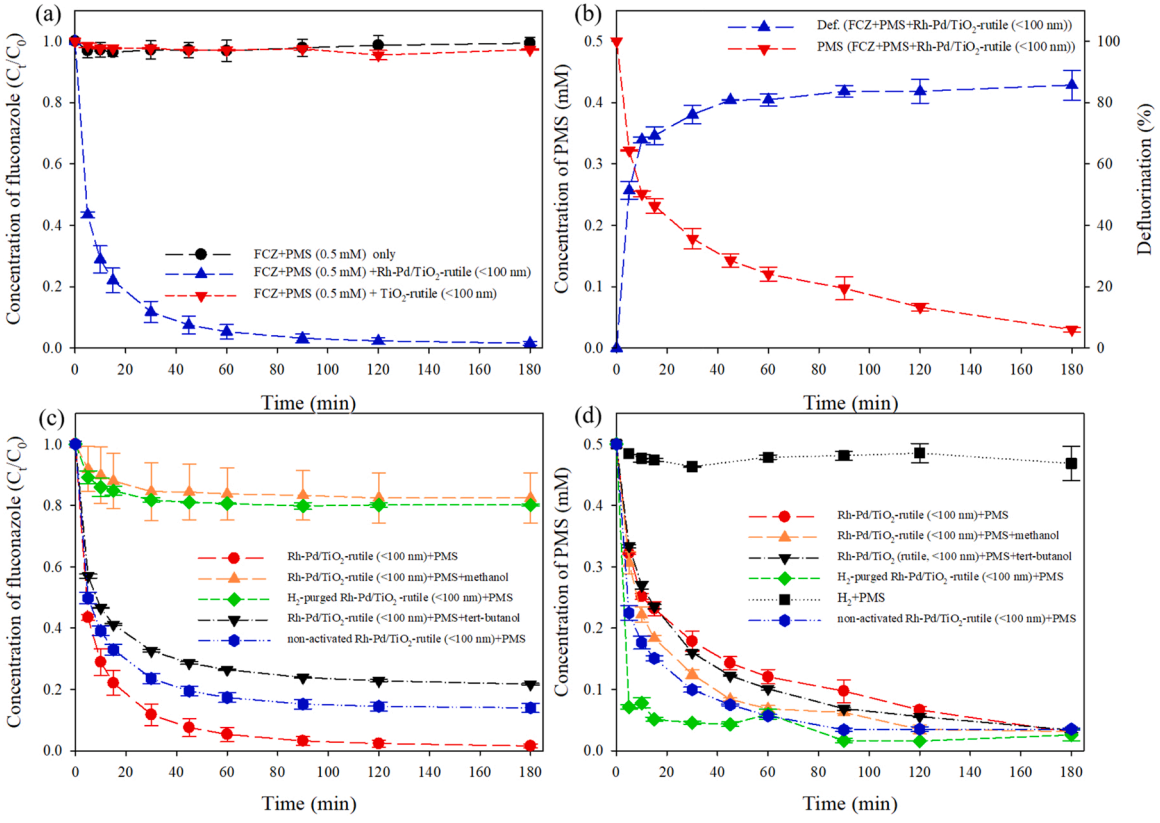

Fig. 2. (a) Oxidative degradation of fluconazole (32.65 μM) by PMS only, TiO_2-rutile (<100 nm), and Rh-Pd/TiO_2-rutile (<100 nm) in the presence of PMS, (b) consumption of PMS and defluorination (%) by Rh-Pd/TiO_2-rutile (<100 nm) during oxidative degradation of fluconazole in (a), (c) effect of methanol and tert-butanol on degradation of fluconazole by Rh-Pd/TiO_2-rutile (<100 nm)/PMS system and oxidation of fluconazole by H_2-purged Rh-Pd/TiO_2-rutile (<100 nm) and nonactivated Rh-Pd/TiO_2-rutile (<100 nm) in the presence of PMS, and (d) time profiles for PMS during the reactions in (c) (Rh = 1%, Pd = 1%, [catalyst] = 0.2 g/L; $[PMS]_0$ = 0.5 mM; [FCZ] = 32.65 μM; $[bicarbonate]_0$ = 0.93 mM; $[methanol]_0/[FCZ]_0$ = 250; $[t\text{-}butanol]_0/[FCZ]_0$ = 250; pH = 7.0).

3.2.2. Role of reactive radicals on fluconazole degradation

To examine the roles of generated $SO_4^{\bullet-}$ and •OH in fluconazole degradation, excess methanol and *tert*-butanol (i.e., $[methanol]_0/[FCZ]_0 = 250$; $[tert\text{-}butanol]_0/[FCZ]_0 = 250$) were added as scavengers of these radicals (Figs. 2c and 2d). Methanol scavenges both $SO_4^{\bullet-}$ ($k = 1.0 \times 10^7$ M^{-1} s^{-1}) and •OH radicals ($k = 9.7 \times 10^8$ M^{-1} s^{-1}, respectively), while *tert*-butanol predominantly scavenges •OH ($k = 3.3 \times 10^9$ M^{-1} s^{-1}) over $SO_4^{\bullet-}$ ($k = 4.0 \times 10^5$ M^{-1} s^{-1}) [45,46]. While methanol significantly inhibited fluconazole degradation, *tert*-butanol only decreased the degradation efficiency from 98.4% to 78.3% over 180 min. Scavenger test suggests that $SO_4^{\bullet-}$ plays more dominant role than •OH for fluconazole oxidation. It is generally known that both $SO_4^{\bullet-}$ and •OH radicals are generated during the PMS activation while $SO_4^{\bullet-}$ is predominantly generated during PDS activation [27]. Therefore, degradation of fluconazole using PDS as oxidant was also investigated and compared with PMS in the presence of the Rh-Pd/TiO_2 catalyst (Fig. A.18). Over 180 min, more than 99% of the fluconazole was degraded with PMS while only 11.2% was degraded with PDS, showing much lower fluconazole removal. These results indicate that our catalyst has better ability for activation of PMS than PDS and generates higher amounts of oxidative radicals leading to higher reactivity with fluconazole.

The influences of metal oxidation states on PMS activation and fluconazole degradation kinetics were also investigated by conducting an experiment using nonactivated Rh-Pd/TiO_2 that contained PdO and Rh_2O_3 as major components (Pd^{2+} = 85.5% and Rh^{3+} = 100%) (Table 2). Compared to activated catalyst having higher metallic Pd and Rh content, nonactivated Rh-Pd/TiO_2 showed slightly slower degradation of fluconazole while higher amount of PMS was consumed (Fig. 2c & 2d) in the same period. For instance, approximately 14% of the initial fluconazole remained even though > 90% PMS was consumed at 90 min (Fig. 2d). These results show that while oxidized form of metals can also activate PMS, metallic Pd and Rh is a more suitable catalyst form that can degrade fluconazole with much efficient PMS utilization.

Degradation of fluconazole was also investigated in the presence of H_{ads}-Pd by purging H_2 (200 mL/min) for 20 min before addition of PMS. Interestingly, the H_2-purged system showed early termination of fluconazole oxidation after 30 min (Fig. 2c). The significance of the inhibitory effect was comparable to that of methanol. The concentration of PMS was monitored as shown in Fig. 2d, where considerable loss of PMS was observed in the H_2-purged system. A control experiment in the absence of Rh-Pd/TiO_2 catalyst was also conducted and showed that PMS loss was negligible in the presence of H_2 alone. These results suggest that a major fraction of PMS reacted with reactive H adsorbed on Pd and Rh nanoparticles (i.e., H_{ads}-Pd and H_{ads}-Rh) and was reduced to sulfate ion at the initial stage of reaction, inhibiting the formation of oxidative radicals. Therefore, removal of H_{ads}-Pd and H_{ads}-Rh from the system is a prerequisite for switching the reaction conditions from reducing to oxidizing to carry out sequential reduction and oxidation of fluconazole by Rh-Pd/TiO_2.

3.2.3. Oxidation intermediates and proposed reaction mechanisms

Radical-induced oxidation of organic compounds can proceed via various reaction mechanisms and produce different intermediates and end-products. Identification of these intermediates is essential for assessing the risk of drug-derived residues in environmental waters and for designing and improving treatment technologies [47]. Oxidation of fluconazole and its associated intermediates by PMS and Rh-Pd/TiO_2 catalysts were investigated using LC–MS and LC-QTOF-MS.

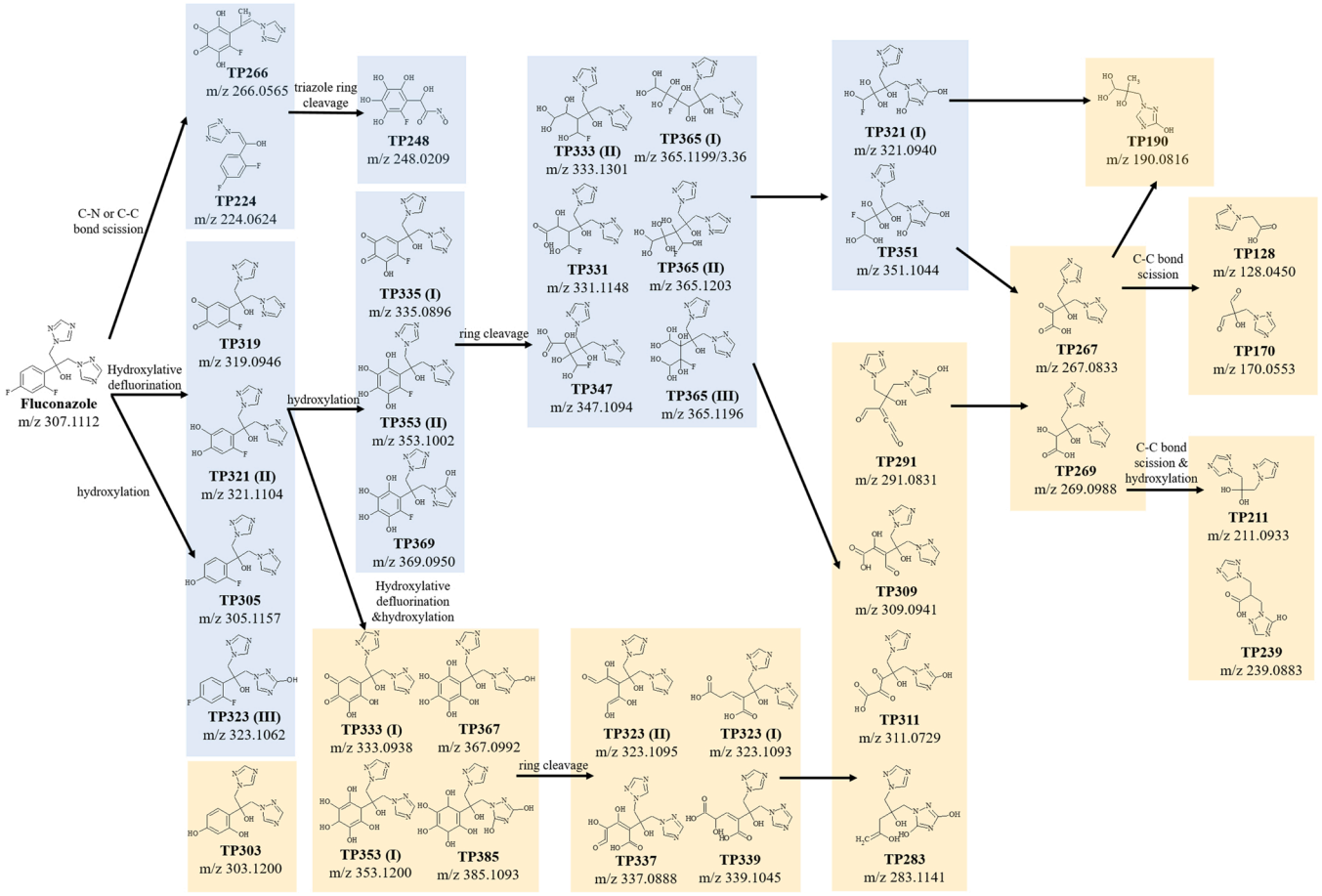

Fig. 3. Pathway for oxidative degradation of fluconazole by Rh-Pd/TiO_2-rutile (<100 nm). Blue and yellow boxes represent fluorinated intermediates and defluorinated intermediates, respectively.

LC-QTOF-MS results provide mass determinations for oxidation intermediates with mass errors lower than 2 ppm (Table A.3), which were used to propose chemical formulas and structures of unknown intermediates with good certainty. Details on intermediate identification from accurate full-product ion spectra obtained by LC-QTOF-MS are provided in the Appendix (Text A.4 and Fig. A.19).

Thirty-eight different transformation products (TPs) were identified during the reaction and are shown in Table A.3 and Fig. 3. All TPs are labeled based on their mass-to-charge ratio (m/z). Likewise, a TP with $[M+H]^+$ ion of m/z 128.0451 was denoted as TP128. Among the 38 TPs, 18 contained at least one fluorine in their structure, indicating that almost half of the total identified oxidation intermediates were still organofluorine compounds (Table A.3). All identified intermediates eluted earlier than fluconazole in reversed-phase liquid chromatography, indicating that these TPs are more hydrophilic than fluconazole. Based on the identified TPs, oxidation of fluconazole with $SO_4^{\bullet-}$ and •OH mainly involved hydroxylation and ring cleavage of fluconazole and its intermediates. Additionally, these compounds can also undergo C-N and/or C-C bond scission and hydroxylative defluorination. Proposed oxidative degradation pathways for fluconazole are summarized in Fig. 3.

Because no reference standards were available for identification of these intermediates, quantification of these TP yields was not possible. Instead, the peak areas of these TPs produced in the selected ion monitoring (SIM) mode of LC–MS analysis were characterized with the kinetic profile of the oxidation process to observe the evolution patterns of each TP during the reaction (Fig. 4). The evolution patterns of 19 TPs are shown in Fig. 4. Other intermediates were not detected, likely due to the lower sensitivity of LC–MS compared to LC-QTOF-MS. Note that the peak response for each ion was different even if other structures were similar; thus, comparisons of peak areas for different TPs should not be used to assess the relative yields of these TPs. Overall, the evolution patterns for the 19 TPs revealed that most of them were produced rapidly, reached peaks at 5–10 min and disappeared as the reaction progressed. Some TPs, such as TP321(I), TP 319, and TP303, showed peaks at 40 min, suggesting that these intermediates were successively formed from initial intermediates of fluconazole oxidation. TP128 also accumulated as the reaction progressed, indicating that TP128 was produced by stepwise oxidation of fluconazole. The evolution patterns of these TPs over time for Rh-Pd/TiO_2, Pd catalyst, and Rh catalyst are provided in Figs. A.20–27.

3.3. Reductive degradation of fluconazole

3.3.1. Degradation kinetics and fluorine removal

Reductive degradation of fluconazole is shown in Fig. 5a. Fluconazole did not degrade under H_2-only conditions, with TiO_2 support only or with monometallic Pd/TiO_2 and Rh/TiO_2 catalysts. Fluconazole reductions were only observed with Rh-Pd/TiO_2 bimetallic catalysts in the presence of H_2. Reductive treatment degraded 71.2±1.7% of the fluconazole in 180 min (Fig. 5a) and gave 56.8±1.7% defluorination (Fig. 5b). The initial reaction exhibited pseudo-first-order reaction kinetics with a rate constant of 0.0191±0.0005 L/(min•g_{cat}). These results indicated that the bimetallic form of Rh-Pd was essential in catalyzing

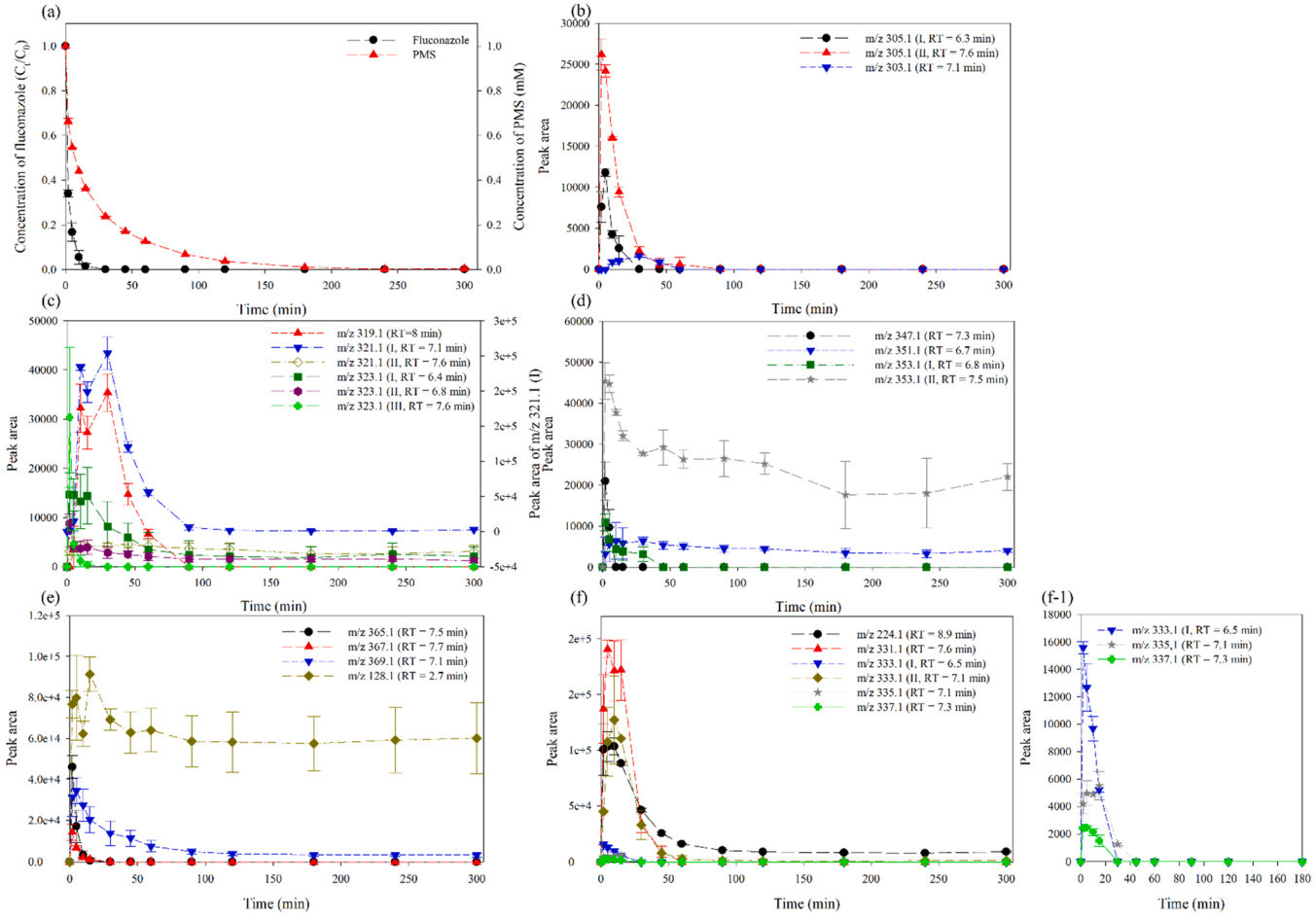

Fig. 4. (a) Oxidative degradation of fluconazole (65.30 μM) by Rh-Pd/TiO_2 (rutile, <100 nm) (Rh = 1% and Pd = 1.5%) in the presence of PMS and reduction of PMS ([catalyst] = 0.4 g/L; $[PMS]_0$ = 1.0 mM; [FCZ] = 65.30 μM; $[bicarbonate]_0$ = 1.0 mM; pH = 3.5±0.1), and (b-f) time profiles for intermediates identified during oxidative degradation of fluconazole in (a). (f-1) magnified profiles of TP333, TP335, and TP337.

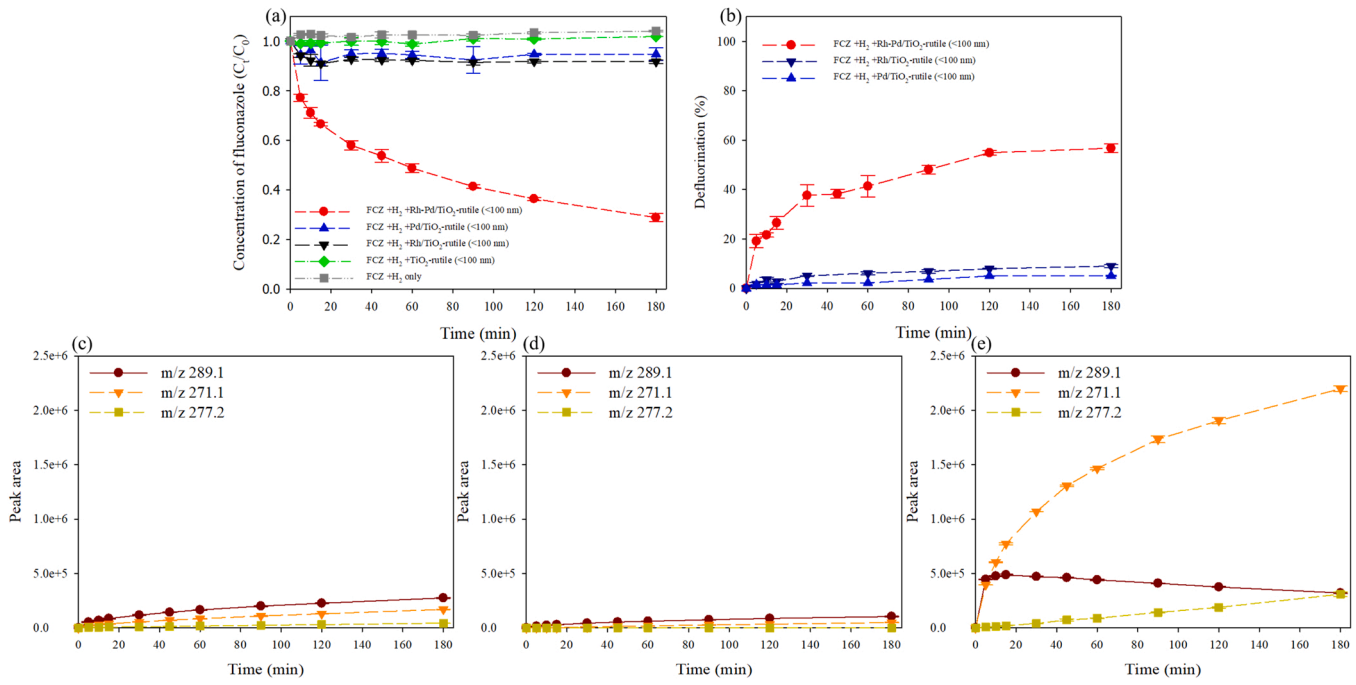

Fig. 5. (a) Reductive degradation of fluconazole by H_2 only, Pd/TiO_2 (rutile, <100 nm), Rh/TiO_2 (rutile, <100 nm), and Rh-Pd/TiO_2 (rutile, <100 nm) (Rh = 1% and Pd = 1%), (b) time profiles of fluconazole defluorination by Pd/TiO_2 (rutile, <100 nm), Rh/TiO2 (rutile, <100 nm), and Rh-Pd/TiO_2 (rutile, <100 nm) (Rh = 1% and Pd = 1%), (c-e) formation of intermediates (TP289, TP271, and TP277) during reductive degradation of fluconazole by (c) Rh/TiO_2 (rutile, <100 nm), (d) Pd/TiO_2 (rutile, <100 nm), and (e) Rh-Pd/TiO_2 (rutile, <100 nm) (H_2 flow rate = 200 mL/min; $[catalyst]_0$ = 0.4 g/L; [FCZ] = 32.65 μM; $[bicarbonate]_0$ = 0.93 mM).

reductive degradation of fluconazole. Moreover, it must be noted that, among all catalysts investigated in this study, only bimetallic Rh-Pd/TiO_2 catalytically oxidized and reduced fluconazole with high reactivity and concurrent defluorination. The influences of metal type (Fig. A.7b), metal loading (Fig. A.28–30), support type (Fig. A.31), initial concentration of fluconazole (Fig. A.16(b)), and NOM (Fig. A.17(b)) on fluconazole reduction were also investigated, and the results as well as detailed discussion are provided in the Appendix A (Text A.5 and A.8). The catalyst used in oxidation experiments was also investigated for its ability to reduce fluconazole (Fig. A.32). The used Rh-Pd/TiO_2 catalyst was found to exhibit about 2.4 times lower reactivity compared to the fresh catalyst for fluconazole reduction. It is possible that catalyst may have been deactivated or a fraction of metals was leached during oxidation reactions. This implies that repeated uses of the catalysts for multiple cycles of oxidation and reduction require a reactivation step.

Changes in Rh and Pd chemical species after fluconazole reduction were also characterized via XPS analysis (Fig. A.5). The ratios of Rh(0) (from 56% to 51%) and Rh^{3+} (from 44% to 49%) did not change significantly after reduction of fluconazole. Similarly, Pd(0) was still predominant after reduction of fluconazole (from 84% to 85%), confirming that these catalysts retained their chemical states during continuous activation by H_2 [24,43].

3.3.2. *Byproduct characterization and proposed reaction mechanism*

The intermediates produced during fluconazole reduction were also characterized, as shown in Table A.4 and Fig. A.33. Three peaks were newly observed with *m/z* 289.1205, 271.1300, and 277.1769, and these corresponded to the proposed chemical formulas $C_{13}H_{13}FN_6O$, $C_{13}H_{14}N_6O$, and $C_{13}H_{20}N_6O$, respectively. These three intermediates are denoted as TP289, TP271, and TP277. As observed in the defluorination profile (Fig. 5b), reductive decomposition of fluconazole entailed direct substitution of F with H. Defluorination of fluconazole resulted in the formation of intermediates TP289 and TP271. Since a difference of *m/z* = 18 indicates to the hydrodefluorination of F (i.e., $[M - F + H]^+$), TP289 and TP271 correspond to loss of one and two fluorine atoms from fluconazole. Accurate full-product ion spectra for TP289, TP271, and TP277 were also collected using LC-QTOF-MS (Fig. A.34). The MS/MS spectrum of TP289 showed a fragmentation pattern similar to that of fluconazole. The product ion at *m/z* 220.0890 (i.e., $C_{11}H_{11}FN_3O^+$) was formed by the loss of $C_2H_3N_3$ (i.e., protonated triazole ring), and the ion at *m/z* 151.0559 (i.e., $C_9H_8FO^+$) was formed by two consecutive losses of $C_2H_3N_3$ from TP289 (i.e., $C_{13}H_{13}FN_6O$). This indicated that one fluorine on the aromatic ring was substituted by H during the catalytic reduction of fluconazole. Another ion at *m/z* 271.1109 was formed by abstraction of H_2O from TP289. Other ions with *m/z* 202.0760 and 182.0738 were formed by losses of H_2O and H_3FO from *m/z* 220.0890. Ions with *m/z* 121.0450 (i.e., C_8H_5F) and *m/z* 70.0417 (i.e., $C_2H_3N_3$) were also identified as fluconazole, indicating that the molecular structure of TP289 was almost identical to that of fluconazole except for the loss of one F. Additionally, we conducted detailed analyses to elucidate the structures of TP271 and TP277 from their full-product ion spectra, which confirmed that TP 271 had lost two F from fluconazole and that TP277 was a hydrogenated derivative of TP 271 (Fig. A.35). Details on the structural identifications of TP271 and TP277 are provided in the Appendix (Text A.9).

The evolution profiles for reduction TPs showed that TP289 was not completely converted to TP271 in the presence of Rh-Pd/TiO_2 within 180 min (Fig. 5c and Fig. A.35), which agreed well with the defluorination profile in Fig. 5b. The peak area of TP277 gradually increased over the course of the reaction (Fig. 5c), suggesting that the catalytic reduction of fluconazole involved (i) reductive conversion of a C-F bond to a C-H bond and (ii) selective hydrogenation of the phenyl group. Similar reductive pathways were observed in our previous study of other fluorinated aromatic compounds [24]. The reductive degradation pathway proposed for fluconazole is shown in Fig. 6a. To investigate additional unidentified intermediates, the initial fluconazole concentration was increased (i.e., $[FCZ]_0$ = 65.30 μM), but no further degradation occurred within 6 h after TP277 was produced (Fig. A.36), which demonstrated that cleavage of the benzene and triazole rings in fluconazole was not induced by the catalytic reduction process.

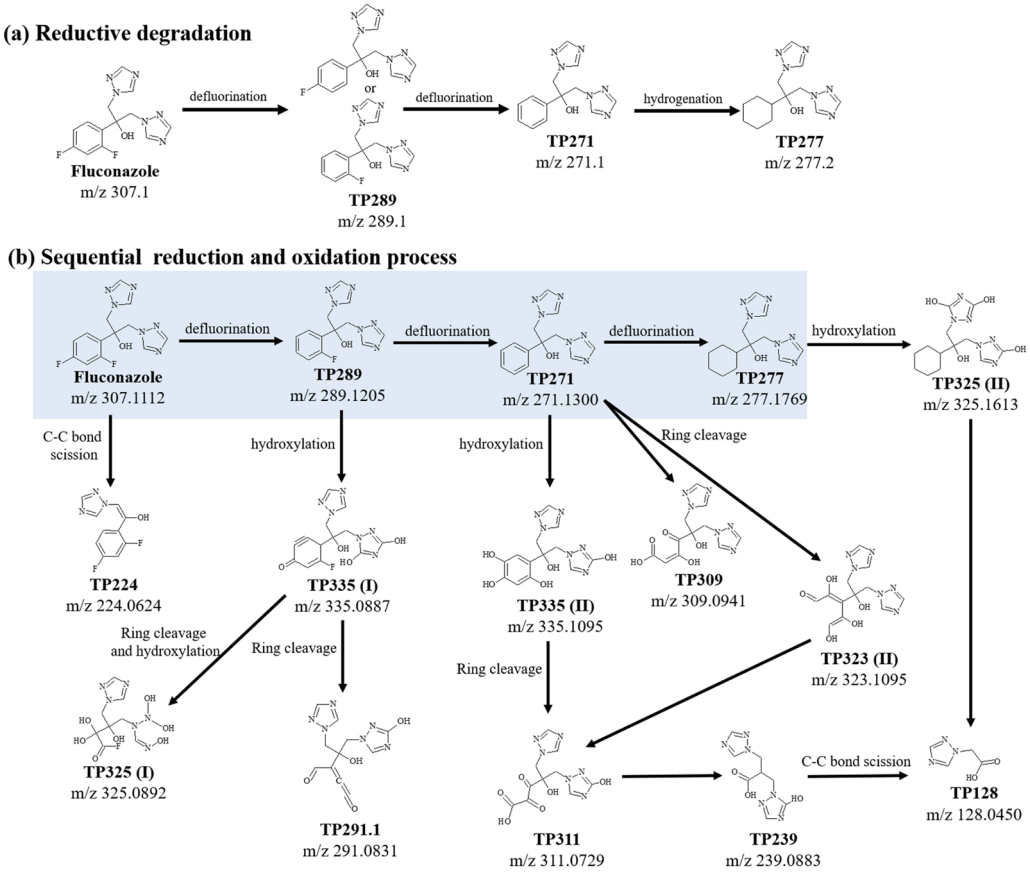

Fig. 6. (a) Pathway for reductive degradation of fluconazole by Rh-Pd/TiO_2 (rutile, <100 nm) and (b) pathway for degradation of fluconazole during sequential reduction and oxidation processes catalyzed by Rh-Pd/TiO_2-rutile (<100 nm). The blue box denotes the reduction pathway for fluconazole.

3.4. Sequential reduction and oxidation of fluconazole

It is worth noting that both catalytic oxidation and reduction efficiently degraded fluconazole. In the oxidation process, generated reactive species ($SO_4^{\bullet-}$ and •OH) attacked the molecular structure of fluconazole and produced many intermediates, including 38 identified TPs; half of these TPs were fluorinated species (Fig. 3). In the reduction process, fluconazole underwent successive hydrodefluorination and hydrogenation reactions of the aromatic ring; however, no further degradation occurred after TP277 (i.e., the intermediate with 2 F removed and the aromatic ring hydrogenated) was formed (Fig. 6a).

To maximize the advantages of the two processes and minimize their drawbacks, sequential reductive and oxidative treatment of fluconazole using Rh-Pd/TiO_2 catalysts was proposed for efficient and safe degradation of the contaminant. Kinetic profiles for fluconazole and key intermediates produced during sequential reduction (i.e., 0–180 min) and oxidation processes (i.e., 180–360 min) are shown in Fig. 7. Over 99% of the fluconazole was degraded with 83.95±1.81% defluorination. As expected, changes in the peak areas for three major intermediates (i.e., TP289, TP271, and TP277) formed during reduction were consistent with the observations previously discussed in Section 3.3, and a continuous increase in fluoride ion content in the solution was observed. At 180 min, the reaction mixture was purged with O_2, and then PMS was immediately spiked into the reactor. O_2 was purged to remove any remaining H_{ads}-Pd^0 and H_{ads}-Rh^0 on the catalyst surface, which would have led to a significant loss of PMS during the initial reaction period. Hence, no PMS loss was observed after O_2 purging (Fig. A.37). PMS addition immediately induced oxidative degradation of the remaining fluconazole. Additionally, TP289, TP271 and TP277 generated during the reductive treatment also underwent oxidative degradation. Almost complete degradation (>99%) of TP289 and TP271 was observed within 15 min of oxidation; while the process was slightly slower, TP277 was also completely oxidized within 30 min (Fig. 7 and Fig. A.37). Defluorination increased from 62.2±3.3% to 80.0±2.2% during the oxidation process, indicating that the remaining fluconazole and TP289 (i.e., $C_{13}H_{13}FN_6O$) underwent hydroxylative defluorination (Fig. 7a). Kinetic profiles for the peak areas of other intermediates produced during oxidation in the sequential treatment were also investigated (Fig. 7b and c). Interestingly, only 11 different TPs were identified with LC-QTOF-MS and LC–MS, which is fewer than the 38 TPs identified for catalytic oxidation alone (described in Section 3.2). Among the 11 TPs, only 3 TPs (i.e., TP311, TP325 (I), and TP 335 (I)) were fluorinated species (Table A.5), likely generated from the remaining fluconazole and TP289. TP224 (i.e., $C_{10}H_7F_2N_3O$) was observed in the sequential redox process, as in the oxidation process, and its formula suggests loss of one triazole ring from fluconazole. Four new TPs were detected for sequential reductive and oxidative treatments. These were TP325 (I) (i.e., *m/z* 325.0892, $C_8H_{13}FN_6O_7$), TP325 (II) (i.e., *m/z* 325.1613, $C_{13}H_{20}N_6O_4$), TP335 (I) (i.e., *m/z* 335.0887, $C_{13}H_{11}FN_6O_4$) and TP335 (II) (i.e., $C_{13}H_{14}N_6O_5$). Moreover, the emergence of penta-, hexa-, and hepta-hydroxylated TP271 identified in the oxidation process was not observed in the sequential reduction and oxidation process. These results suggested that (i) the oxidative degradation pathway was significantly changed when defluorinated TPs were provided as new substrates for post-oxidation steps, (ii) the formation of fluorinated TPs was suppressed, and (iii) the number of TPs was significantly reduced from 38 to 11 during sequential reduction–oxidation of fluconazole by Rh-Pd/TiO_2. A detailed investigation of MS/MS spectra for the newly identified TPs is presented in Fig. A.38. Based on the results, a proposed degradation pathway for sequential reduction and oxidation of fluconazole is presented in Fig. 6b. Notably, TP325(II) was formed via tri-hydroxylation of TP277, confirming that TP277 was provided as a new substrate for

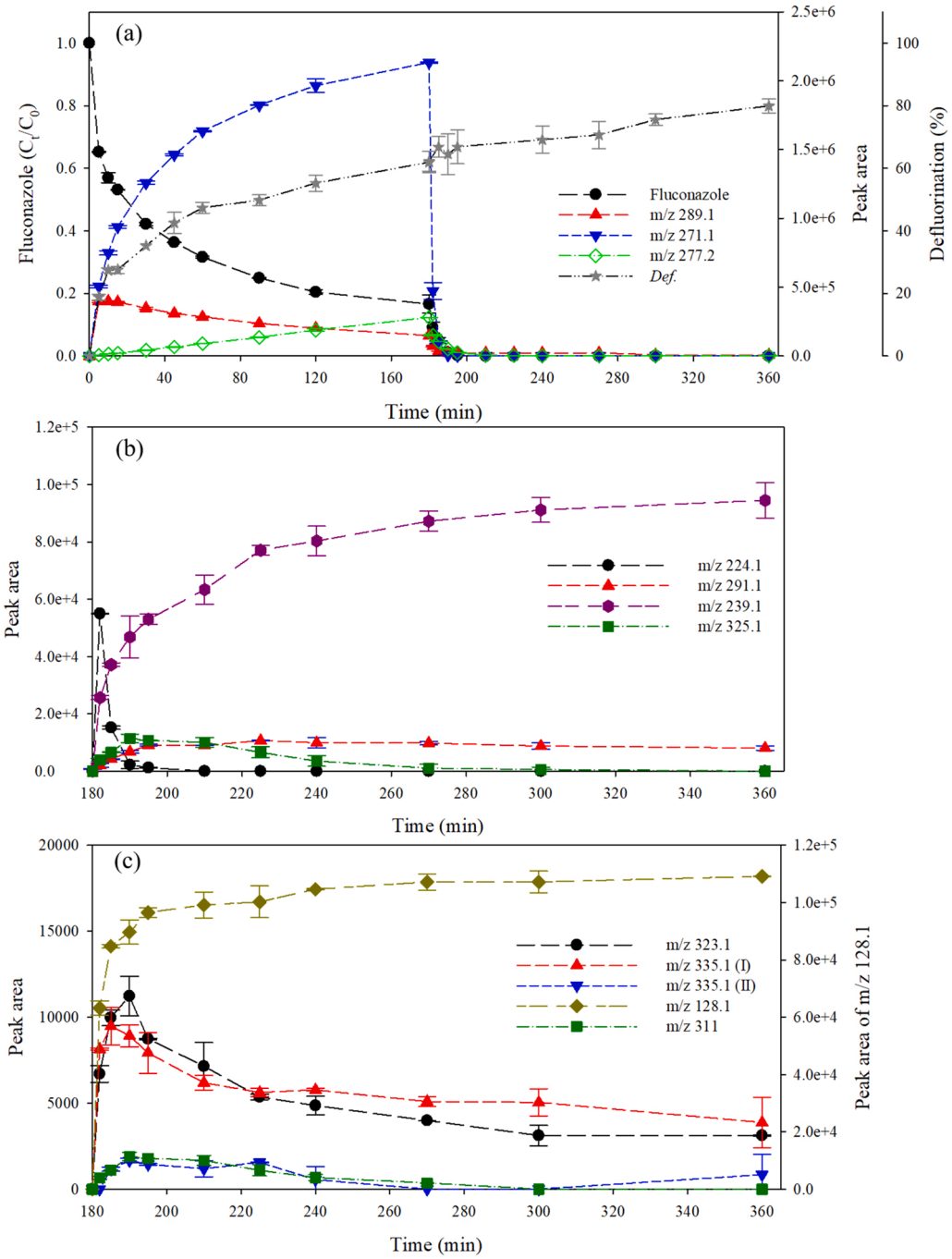

Fig. 7. (a) Sequential reduction and oxidation of fluconazole by Rh-Pd/TiO_2 (rutile, <100 nm) and formation of major intermediates (TP289, TP271, and TP277). (H_2 flow rate = 200 cc/min; $[catalyst]_0$ = 0.4 g/L; $[PMS]_0$ = 1.0 mM; [FCZ] = 32.65 μM). (b-c) Time profiles for identified intermediates (i.e., TP128, TP224, TP239, TP291, TP323, TP325, TP335(I), and TP335(II)).

oxidative treatment by Rh-Pd/TiO_2. Similarly, TP335 (I) could be generated by the combination of tri-hydroxylation and hydrogen abstraction from TP289. An opened ring structure was also identified for TP325 (I), TP291, TP311, and TP309. In addition, TP239 and TP128 were also identified, confirming the complete removal of aromatic rings and subsequent loss of triazole rings. Both TP239 and TP128 accumulated as the oxidation reaction proceeded (Fig. 7b and c).

Intermediates produced in the three processes are compared in Fig. 8. This shows that sequential reduction and oxidation processes for abatement of fluconazole significantly reduced the number of TPs compared to the oxidation process alone. The formation of 18 TPs containing F which are observed in single oxidation process was greatly suppressed in the sequential reduction and oxidation process (i.e., 3 fluorinated TPs only). This signified that pre-removal of F in reduction step contributed to reducing the number of fluorinated TPs in post-oxidation step. But the number of defluorinated TPs in the sequential process (i.e., 10 defluorinated TPs) was also lower compared to single oxidation process (i.e., 20 defluorinated TPs). Therefore, to further elucidate this phenomenon, DFT calculations were conducted to predict reactive sites of fluconazole and defluorinated TPs (i.e., TP289, TP271, and TP277). The difference of reactive sites between oxidation process and the sequential process will be discussed in the next section.

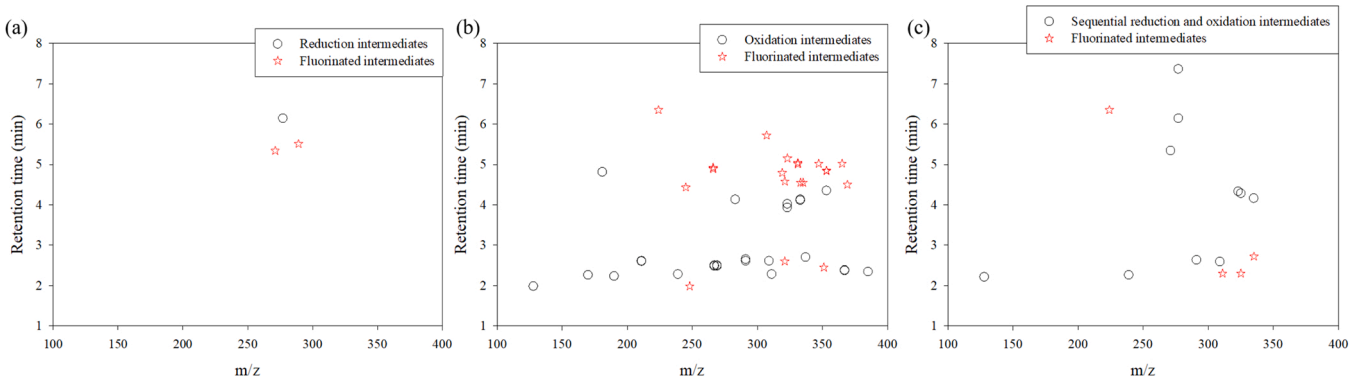

Fig. 8. Scatter plots for identified TPs: (a) catalytic reduction, (b) oxidation, and (c) sequential reduction and oxidation of fluconazole. A star indicates fluorinated species.

3.5. DFT calculations of fluconazole and intermediate products

The reactive sites of fluconazole were investigated computationally using the HOMO, LUMO and Fukui functions (Figs. A.39–41 and Table A.6–9). The chemical structure of fluconazole with a condensed version of the Fukui function (i.e., f^- values) for atoms is presented in Fig. 9a. A higher f^- indicates that the site is more susceptible to electrophilic attack by oxidants. For fluconazole, f^- values higher than 0.05 were obtained for C_1, C_2, C_5, C_{25}, and F_{33} in the difluorophenyl group and one azole group, suggesting that these are likely to be primary sites for reactions with •OH and $SO_4^{\bullet-}$ radicals [39]. The next group comprising N_{23}, N_{24}, C_{26}, F_{34} showed values higher than 0.04. The last group with C_3 (0.033), C_4 (0.037), and C_6 (0.022) exhibited lower values than other C sites in the difluorophenyl group. Oxidative attack at C_3, C_4, and C_6 might not be preferred compared to attack at atoms with $f^- >$ 0.04 in fluconazole. After hydroxylative defluorination and hydroxylation (i.e., formation of TP321 (II)), the f^- values of C4 increased to 0.076, and C_3 and C_6 became close to 0.04 (Fig. A.42). Thus, they became preferred sites for electrophilic attack. Specifically, radical attacks of these sites induced (i) mono-hydroxylation of C_{25} to form TP323 (III), (ii) hydroxylative defluorination of F_{33} and F_{34} to form TP305 and TP303, (iii) a combination of hydroxylation and hydroxylative defluorination of C_1 and F_{33} to form TP321 (II) and TP319, (iv) di-hydroxylation of C_1 and C_3, hydroxylative defluorination of C_2-F_{33}, and hydrogen abstraction to form TP335 (I), (v) hydroxylative defluorination of F_{33} and tri-hydroxylation of C_1, C_2, and C_3 to form TP353 (II), and (vi) hydroxylative defluorination of F_{33} and tetra-hydroxylation of C_1, C_2, C_3, and C_{25} to form TP369, (vii) hydroxylative defluorination of F_{34} and hydroxylation of C_{26} in TP353 (II) to form TP367, and (viii) hydroxylative defluorination of F_{33} and F_{34} and penta-hydroxylation of C_1, C_3, C_6, C_{25}, and C_{26} to form TP385. It was demonstrated that fluconazole has multiple reactive sites for oxidative radicals, and therefore, it is difficult to force fluconazole to proceed via specific degradation pathways during oxidative treatment; oxidative treatment results in the formation of a large number of TPs, including some that are fluorinated. These DFT results were in good agreement

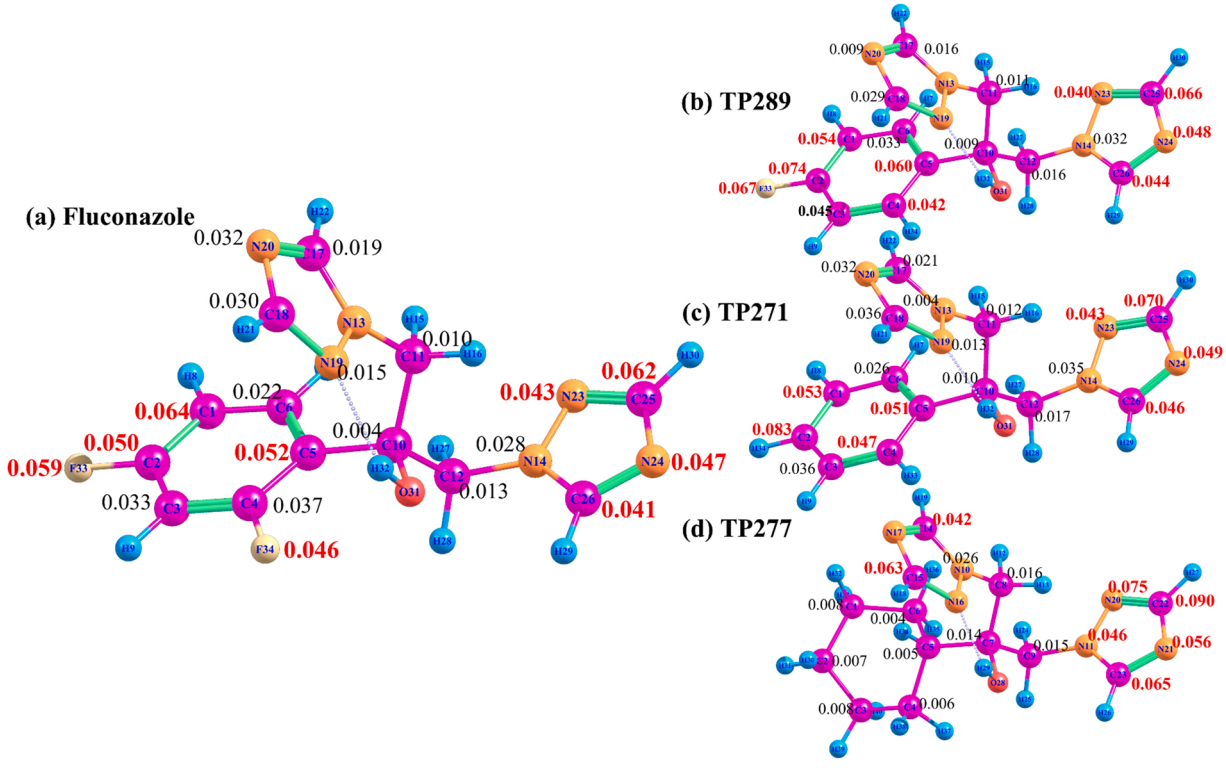

Fig. 9. Condensed Fukui function for electrophilic attack (f^-) on (a) fluconazole, (b) TP289, (c) TP271, and (d) TP277.

with the experimental results for oxidative degradation as discussed in Section 3.2.3, indicating that the proposed oxidative degradation pathway determined by f^- is reliable.

For the sequential reduction and oxidation of fluconazole, defluorinated TPs (i.e., TP289, TP271, and TP277) produced from catalytic reduction undergo post-oxidative degradation. Hence, additional DFT calculations were performed on TP289, TP271 and TP277 (Table A.6–9). Reductive defluorination of F_{33} and F_{34} from fluconazole resulted in an increase in f^- for C_2 (from 0.050 to 0.083), C_4 (0.037–0.047), C_{25} (0.062–0.070), and C_{26} (0.041–0.046) on going from fluconazole to TP271. These results suggested that reductive conversion of C-F to C-H renders the specific carbon sites on the phenyl group more vulnerable to radical attack. For TP277, f^- values for C_{14} and C_{15} in the second triazole group were also significantly increased. While TP277 is not a dominant TP generated during the reduction reaction, it could promote destruction of triazole groups (e.g., TP325 (I)) in fluconazole during the subsequent oxidation step. We also calculated the HOMO and LUMO of fluconazole (Fig. A.39) and its reductive intermediates, and similar results were observed as those from the Fukui function (Text A.10).

As mentioned in Section 3.4, the degradation pathways of fluconazole in oxidation and sequential redox processes were different. The sequential reduction and oxidation of fluconazole reduced the number of TPs and suppressed the formation of fluorinated species. From experimental and computational analyses, it is proposed that i) reductive defluorination of F_{33} and F_{34} made radical attack on benzene and the two adjacent triazole rings more likely, and ii) the stability of the two triazole rings decreased after hydrogenation of the benzene ring. The formation of fluorinated intermediates during oxidative treatments of organofluorine compounds is an important challenge to overcome. Therefore, sequential catalytic reduction and oxidation processes may provide useful insights for abatement of fluorinated pharmaceuticals in aqueous media through safe degradation pathways.

4. Conclusion

This study investigated for the first time the applicability of bimetallic catalysts used for both reductive hydrogenation and radical-based advanced oxidation in the treatment of fluorinated drugs. Key findings from this study are:

- Rh-Pd bimetallic catalysts on TiO_2-rutile supports were successfully synthesized, and a series of characterization techniques revealed that Rh and Pd metals were in close proximity and that their ensembles were highly dispersed on the TiO_2 surface.
- Using a fluorinated pharmaceutical (i.e., fluconazole) as a target contaminant, the Rh-Pd/TiO_2-rutile catalysts enabled catalytic oxidation via Rh- and Pd-activated •OH and $SO_4^{\bullet-}$. However, catalytic oxidation of fluconazole utilized multiple oxidation pathways resulting in the formation of 38 different TPs, among which 18 TPs were still fluorinated.
- The same catalyst successfully catalyzed reductive degradation of fluconazole in the presence of H_2. The reductive pathways were predominantly defluorination and hydrogenation, and no further degradation was observed.
- Catalytic reduction followed directly by oxidation in a single reactor using the same Rh-Pd/TiO_2 catalysts provided improved efficiency for degradation of fluconazole and generated a smaller number of TPs overall as well as a smaller number of fluorinated TPs. The differences between catalytic oxidative and reductive pathways were also investigated via DFT calculations, which identified primary reactive sites in fluconazole and its intermediates.

The insights obtained from this study are valuable for abatement of fluorinated pharmaceuticals, in which efficient treatment of the parent compound as well as minimal formation of fluorine-containing intermediates are both important. While future research is needed for design and development of reactors (such as sequential batch reactors or continuous flow reactors) and treatment processes (such as better utilization of H_2 or PMS) that utilize these catalysts in sequential and/or simultaneous oxidative and reductive reactions, the results of this study open up new and promising possibilities for the use of a single catalyst triggering both oxidative and reductive treatments, which is useful not just for removal of fluorinated pharmaceuticals but also for other organic contaminants in aqueous media.

CRediT authorship contribution statement

Jaehyeong Park: Conceptualization, Methodology, Investigation, Formal analysis, Visualization, Writing – original draft. **Sungjun Bae**: Investigation, Formal analysis, Visualization, Writing – review & editing. **Yongju Choi**: Investigation, Formal analysis, Writing – review & editing. **Jong Kwon Choe**: Conceptualization, Methodology, Resources, Writing – original draft, Writing – review & editing, Supervision, Funding acquisition.

Declaration of Competing Interest

The authors declare that they have no known competing financial interests or personal relationships that could have appeared to influence the work reported in this paper.

Data availability

Data will be made available on request.

Acknowledgments

This work was supported by the National Research Foundation of Korea (NRF- 2020R1C1C1006228 and NRF-2021R1A4A1026364). It is also supported by the BK21 PLUS research program of NRF and Institute of Engineering Research at SNU.

Appendix A. Supporting information

Supplementary data associated with this article can be found in the online version at doi:10.1016/j.apcatb.2022.122089.

References

[1] M. Inoue, Y. Sumii, N. Shibata, Contribution of organofluorine compounds to pharmaceuticals, ACS Omega 5 (2020) 10633–10640, https://doi.org/10.1021/acsomega.0c00830.
[2] T. Furuya, A.S. Kamlet, T. Ritter, Catalysis for fluorination and trifluoromethylation, Nature 473 (2011) 470–477, https://doi.org/10.1038/nature10108.
[3] Y. Ogawa, E. Tokunaga, O. Kobayashi, K. Hirai, N. Shibata, Current contributions of organofluorine compounds to the agrochemical industry, IScience 23 (2020), 101467, https://doi.org/10.1016/j.isci.2020.101467.
[4] T. Fujiwara, D. O'Hagan, Successful fluorine-containing herbicide agrochemicals, J. Fluor. Chem. 167 (2014) 16–29, https://doi.org/10.1016/j.jfluchem.2014.06.014.
[5] E.M.S, T.M. Swager, Fluorofluorophores: fluorescent fluorous chemical tools spanning the visible spectrum, Org. Chem. ((2014) 13574–13577.
[6] E. Heath, T. Kosjek, C.Á. Diazepam, Á.E.Á. Halogenated, Sources, Occur. Fate Halog. Heterocycl. Pharm. Environ. (2012) 247–268, https://doi.org/10.1007/7081.
[7] M.G. Antoniou, G. Hey, S. Rodríguez Vega, A. Spiliotopoulou, J. Fick, M. Tysklind, J. la Cour Jansen, H.R. Andersen, Required ozone doses for removing pharmaceuticals from wastewater effluents, Sci. Total Environ. 456–457 (2013) 42–49, https://doi.org/10.1016/j.scitotenv.2013.03.072.
[8] M. Sörengård, H. Campos-Pereira, M. Ullberg, F.Y. Lai, O. Golovko, L. Ahrens, Mass loads, source apportionment, and risk estimation of organic micropollutants from hospital and municipal wastewater in recipient catchments, Chemosphere 234 (2019) 931–941, https://doi.org/10.1016/j.chemosphere.2019.06.041.
[9] J. Kim, H. Jang, J. Kim, H. Ishibashi, M. Hirano, K. Nasu, N. Ichikawa, Y. Takao, R. Shinohara, K. Arizono, Occurrence of Pharmaceutical and Personal Care

Products (PPCPs) in Surface Water from Mankyung River, South Korea, J. Heal. Sci. 55 (2009) 249–258.
[10] Z.F. Chen, G.G. Ying, Y.X. Jiang, B. Yang, H.J. Lai, Y.S. Liu, C.G. Pan, F.Q. Peng, Photodegradation of the azole fungicide fluconazole in aqueous solution under UV-254: Kinetics, mechanistic investigations and toxicity evaluation, Water Res 52 (2014) 83–91, https://doi.org/10.1016/j.watres.2013.12.039.
[11] M. Hörsing, T. Kosjek, H.R. Andersen, E. Heath, A. Ledin, Fate of citalopram during water treatment with O3, ClO2, UV and fenton oxidation, Chemosphere 89 (2012) 129–135, https://doi.org/10.1016/j.chemosphere.2012.05.024.
[12] R. Bai, W. Yan, Y. Xiao, S. Wang, X. Tian, J. Li, X. Xiao, X. Lu, F. Zhao, Acceleration of peroxymonosulfate decomposition by a magnetic MoS2/CuFe2O4 heterogeneous catalyst for rapid degradation of fluoxetine, Chem. Eng. J. 397 (2020), 125501, https://doi.org/10.1016/j.cej.2020.125501.
[13] F. Méndez-Arriaga, T. Otsu, T. Oyama, J. Gimenez, S. Esplugas, H. Hidaka, N. Serpone, Photooxidation of the antidepressant drug Fluoxetine (Prozac®) in aqueous media by hybrid catalytic/ozonation processes, Water Res 45 (2011) 2782–2794, https://doi.org/10.1016/j.watres.2011.02.030.
[14] Y. Zhao, G. Yu, S. Chen, S. Zhang, B. Wang, J. Huang, S. Deng, Y. Wang, Ozonation of antidepressant fluoxetine and its metabolite product norfluoxetine: Kinetics, intermediates and toxicity, Chem. Eng. J. 316 (2017) 951–963, https://doi.org/10.1016/j.cej.2017.02.032.
[15] I. Epold, M. Trapido, N. Dulova, Degradation of levofloxacin in aqueous solutions by Fenton, ferrous ion-activated persulfate and combined Fenton / persulfate systems, Chem. Eng. J. 279 (2015) 452–462, https://doi.org/10.1016/j.cej.2015.05.054.
[16] W.W. Cai, T. Peng, B. Yang, C. Xu, Y.S. Liu, J.L. Zhao, F.L. Gu, G.G. Ying, Kinetics and mechanism of reactive radical mediated fluconazole degradation by the UV/chlorine process: Experimental and theoretical studies, Chem. Eng. J. 402 (2020), https://doi.org/10.1016/j.cej.2020.126224.
[17] H. Guo, N. Gao, W. Chu, Photochemical degradation of ciprofloxacin in UV and UV/H2O 2 process: kinetics, parameters, and products, Environ. Sci. Pollut. Res. 20 (2013) 3202–3213, https://doi.org/10.1007/s11356-012-1229-x.
[18] S.K. Kansal, P. Kundu, S. Sood, R. Lamba, A. Umar, S.K. Mehtab, Photocatalytic degradation of the antibiotic levofloxacin using highly crystalline TiO2, N. J. Chem. 38 (2014) 3220–3226, https://doi.org/10.1039/c3nj01619f.
[19] D. Nasuhoglu, A. Rodayan, D. Berk, V. Yargeau, Removal of the antibiotic levofloxacin (LEVO) in water by ozonation and TiO2 photocatalysis, Chem. Eng. J. 189–190 (2012) 41–48, https://doi.org/10.1016/j.cej.2012.02.016.
[20] C. Salazar, C. Ridruejo, E. Brillas, J. Yáñez, H.D. Mansilla, I. Sirés, Abatement of the fluorinated antidepressant fluoxetine (Prozac) and its reaction by-products by electrochemical advanced methods, Appl. Catal. B Environ. 203 (2017) 189–198, https://doi.org/10.1016/j.apcatb.2016.10.026.
[21] H. Yang Shao, M. Hong Wu, F. Deng, G. Xu, N. Liu, X. Li, L. Tang, Electron beam irradiation induced degradation of antidepressant drug fluoxetine in water matrices, Chemosphere 190 (2018) 184–190, https://doi.org/10.1016/j.chemosphere.2017.09.133.
[22] A.S. Giri, A.K. Golder, Ciprofloxacin degradation from aqueous solution by Fenton oxidation: Reaction kinetics and degradation mechanisms, RSC Adv. 4 (2014) 6738–6745, https://doi.org/10.1039/c3ra45709e.
[23] B.C. Hodges, E.L. Cates, J.H. Kim, Challenges and prospects of advanced oxidation water treatment processes using catalytic nanomaterials, Nat. Nanotechnol. 13 (2018) 642–650, https://doi.org/10.1038/s41565-018-0216-x.
[24] J. Park, S. An, E.H. Jho, S. Bae, Y. Choi, J.K. Choe, Exploring reductive degradation of fluorinated pharmaceuticals using Al2O3-supported Pt-group metallic catalysts: Catalytic reactivity, reaction pathways, and toxicity assessment, Water Res (2020), 116242, https://doi.org/10.1016/j.watres.2020.116242.
[25] R. Baumgartner, G.K. Stieger, K. McNeill, Complete hydrodehalogenation of polyfluorinated and other polyhalogenated benzenes under mild catalytic conditions, Environ. Sci. Technol. 47 (2013) 6545–6553, https://doi.org/10.1021/es401183v.
[26] R. Baumgartner, K. McNeill, Hydrodefluorination and hydrogenation of fluorobenzene under mild aqueous conditions, Environ. Sci. Technol. 46 (2012) 10199–10205, https://doi.org/10.1021/es302188f.
[27] Y. Feng, P. Lee, D. Wu, K. Shih, Surface-bound sulfate radical-dominated degradation of 1, 4-dioxane by alumina-supported palladium (Pd/Al2O3) catalyzed peroxymonosulfate, Water Res 120 (2017) 12–21, https://doi.org/10.1016/j.watres.2017.04.070.
[28] Y.Y. Ahn, E.T. Yun, J.W. Seo, C. Lee, S.H. Kim, J.H. Kim, J. Lee, Activation of Peroxymonosulfate by Surface-Loaded Noble Metal Nanoparticles for Oxidative Degradation of Organic Compounds, Environ. Sci. Technol. 50 (2016) 10187–10197, https://doi.org/10.1021/acs.est.6b02841.
[29] Y.Y. Ahn, H. Bae, H. Il Kim, S.H. Kim, J.H. Kim, S.G. Lee, J. Lee, Surface-loaded metal nanoparticles for peroxymonosulfate activation: Efficiency and mechanism reconnaissance, Appl. Catal. B Environ. 241 (2019) 561–569, https://doi.org/10.1016/j.apcatb.2018.09.056.
[30] J. Jung, S. Bae, W. Lee, Nitrate reduction by maghemite supported Cu-Pd bimetallic catalyst, Appl. Catal. B Environ. 127 (2012) 148–158, https://doi.org/10.1016/j.apcatb.2012.08.017.
[31] C. Liang, C.F. Huang, N. Mohanty, R.M. Kurakalva, A rapid spectrophotometric determination of persulfate anion in ISCO, Chemosphere 73 (2008) 1540–1543, https://doi.org/10.1016/j.chemosphere.2008.08.043.
[32] F. Neese, The ORCA program system, Wiley Interdiscip, Rev. Comput. Mol. Sci. 2 (2012) 73–78, https://doi.org/10.1002/wcms.81.
[33] P.M.W. Gill, B.G. Johnson, J.A. Pople, M.J. Frisch, The performance of the Becke-Lee-Yang-Parr (B-LYP) density functional theory with various basis sets, Chem. Phys. Lett. 197 (1992) 499–505, https://doi.org/10.1016/0009-2614(92)85807-M.
[34] A. Schäfer, H. Horn, R. Ahlrichs, Fully optimized contracted Gaussian basis sets for atoms Li to Kr, J. Chem. Phys. 97 (1992) 2571–2577, https://doi.org/10.1063/1.463096.
[35] Marcus D. Hanwell1, Donald ECurtis, D.C. Lonie, T. Vandermeersch, E. Zurek, G. R. Hutchison, Avogadro: an advanced semantic chemical editor, visualization, and analysis platform, Adv. Math. (N. Y) 262 (2014) 476–483, https://doi.org/10.1016/j.aim.2014.05.019.
[36] Y. Li, Y. Yang, J. Lei, W. Liu, M. Tong, J. Liang, The degradation pathways of carbamazepine in advanced oxidation process: A mini review coupled with DFT calculation, Sci. Total Environ. 779 (2021), 146498, https://doi.org/10.1016/j.scitotenv.2021.146498.
[37] B. De Witte, H. Van Langenhove, K. Hemelsoet, K. Demeestere, P. De Wispelaere, V. Van Speybroeck, J. Dewulf, Levofloxacin ozonation in water: Rate determining process parameters and reaction pathway elucidation, Chemosphere 76 (2009) 683–689, https://doi.org/10.1016/j.chemosphere.2009.03.048.
[38] M. Ma, L. Chen, J. Zhao, W. Liu, H. Ji, Efficient activation of peroxymonosulfate by hollow cobalt hydroxide for degradation of ibuprofen and theoretical study, Chin. Chem. Lett. 30 (2019) 2191–2195, https://doi.org/10.1016/j.cclet.2019.09.031.
[39] P. Geerlings, F. De Proft, W. Langenaeker, Conceptual density functional theory, Chem. Rev. 103 (2003) 1793–1873, https://doi.org/10.1021/cr990029p.
[40] N. Ammouchi, H. Allal, Y. Belhocine, S. Bettaz, E. Zouaoui, DFT computations and molecular dynamics investigations on conformers of some pyrazinamide derivatives as corrosion inhibitors for aluminum, J. Mol. Liq. 300 (2020), 112309, https://doi.org/10.1016/j.molliq.2019.112309.
[41] N. Ammouchi, H. Allal, Y. Belhocine, S. Bettaz, E. Zouaoui, DFT computations and molecular dynamics investigations on conformers of some pyrazinamide derivatives as corrosion inhibitors for aluminum, J. Mol. Liq. 300 (2020), 112309, https://doi.org/10.1016/j.molliq.2019.112309.
[42] Y. Xie, H. Cao, Y. Li, Y. Zhang, J.C. Crittenden, Highly Selective PdCu/Amorphous Silica À Alumina (ASA) Catalysts for Groundwater Denitration, Environ. Sci. Pollut. Res 45 (2011) 4066–4072, https://doi.org/10.1021/es104050h.
[43] S. Hamid, M.A. Kumar, W. Lee, Highly reactive and selective Sn-Pd bimetallic catalyst supported by nanocrystalline ZSM-5 for aqueous nitrate reduction, Appl. Catal. B Environ. 187 (2016) 37–46, https://doi.org/10.1016/j.apcatb.2016.01.035.
[44] J. Park, S. Bae, Highly efficient and magnetically recyclable Pd catalyst supported by iron-rich fly ash@fly ash-derived SiO2 for reduction of p-nitrophenol, J. Hazard. Mater. 371 (2019) 72–82, https://doi.org/10.1016/j.jhazmat.2019.02.105.
[45] G.V. Buxton, C.L. Greenstock, W.P. Helman, A.B. Ross, Critical Review of rate constants for reactions of hydrated electrons, hydrogen atoms and hydroxyl radicals (·OH/·O−in Aqueous Solution, J. Phys. Chem. Ref. Data (1988), https://doi.org/10.1063/1.555805.
[46] C.L. Clifton, R.E. Huie, Rate constants for some hydrogen abstraction reactions of the carbonate radical, Int. J. Chem. Kinet. 25 (1993) 199–203, https://doi.org/10.1002/kin.550250308.
[47] D. Lambropoulou, E. Evgenidou, V. Saliverou, C. Kosma, I. Konstantinou, Degradation of venlafaxine using TiO2/UV process: Kinetic studies, RSM optimization, identification of transformation products and toxicity evaluation, J. Hazard. Mater. 323 (2017) 513–526, https://doi.org/10.1016/j.jhazmat.2016.04.074.